Applied Catalysis B: Environmental 197 (2016) 262–270

Contents lists available at ScienceDirect

Applied Catalysis B: Environmental

journal homepage: www.elsevier.com/locate/apcatb

High efficiency of Pt^{2+}- CeO_2 novel thin film catalyst as anode for proton exchange membrane fuel cells

Roman Fiala[a], Alberto Figueroba[b], Albert Bruix[c], Michal Vaclavu[a], Andrii Rednyk[a], Ivan Khalakhan[a], Mykhailo Vorokhta[a], Jaroslava Lavkova[a,d], Francesc Illas[b], Valerie Potin[d], Iva Matolinova[a], Konstantin M. Neyman[b,e,**], Vladimir Matolin[a,*]

[a] Charles University in Prague, Faculty of Mathematics and Physics, Department of Surface and Plasma Science, V Holešovičkách 2, 18000 Prague, Czech Republic
[b] Departament de Química Física and Institut de Química Teòrica i Computacional (IQTCUB), Universitat de Barcelona, c/Martí i Franquès 1, 08028 Barcelona, Spain
[c] Department of Physics and Astronomy and Interdisciplinary Nanoscience Center, Aarhus University, Ny Munkegade 120, Building 1520, DK-8000 Aarhus, Denmark
[d] Laboratoire Interdisciplinaire Carnot de Bourgogne, UMR 6303CNRS-Université de Bourgogne, 9 Av. A. Savary, BP 47870, F-21078 Dijon Cedex, France
[e] Institucio Catalana de Recerca i Estudis Avançats (ICREA), 08010 Barcelona, Spain

ARTICLE INFO

Article history:
Received 29 November 2015
Received in revised form 2 February 2016
Accepted 16 February 2016
Available online 20 February 2016

Keywords:
Platinum
Cerium oxide
Fuel cell
Thin film

ABSTRACT

The elevated price of Pt limits the large-scale implementation of commercial proton exchange membrane fuel cells, which effectively convert chemical energy into electricity. In order to increase the cost-efficiency in proton-exchange membrane fuel cells, we have designed a family of novel anode catalysts consisting of thin films of ceria with low Pt loadings sputtered on a nanostructured carbon support. Remarkably, only such small amounts of Pt are necessary for achieving power density values comparable to the reference commercial catalysts, which results in excellent specific activities of our samples. By combining photoelectron spectroscopy and catalytic performance analysis, we have shown that the surface Pt^{2+} species in cerium oxide exhibit high electrocatalytic activity. Density functional theory calculations show that the great stability of Pt^{2+} species on ceria makes these resistant to reduction by hydrogenation and suggests that the formation of such stable surface complexes prevents degradation of the nanostructured composite.

1. Introduction

Fuel cells (FC) directly convert chemical energy into electricity and are nowadays widely regarded as one of the key energy solutions for the 21st century. In particular, proton exchange membrane fuel cells (PEMFC) are considered as the most promising systems for mobile systems powering. These devices use Pt-containing materials as catalysts, and the excessive cost of this precious metal constitutes a major obstacle limiting the large-scale commercialization of their applications. In fact, reducing the demand for Pt and other precious metals is one of driving forces in catalysis research. For that one either replaces the precious metals by less expensive alternatives or strives to use these precious metals as efficiently as possible. The latter approach commonly involves substantial increase of the metal dispersion with a concomitantly increasing the number of metal sites accessible to reactants. Alternatively, one may change the chemical state (i.e. the oxidation state) of such metals to enhance the catalytic activity of each metal site, at least towards some reactions [1]. The combination of these two concepts in the preparation of atomically dispersed metal-catalysts featuring highly active chemical states, thus, represents a very attractive strategy for increasing noble metal efficiency. Nevertheless, the preparation of such ideal catalytic material must also stabilize the active phase against sintering and bulk diffusion, since these processes dramatically lower the number of available metal sites at the surface of the catalyst.

* Corresponding author.
** Corresponding author at: Departament de Química Física and Institut de Química Teòrica i Computacional (IQTCUB), Universitat de Barcelona, c/Martí i Franquès 1, 08028 Barcelona, Spain.
E-mail addresses: konstantin.neyman@icrea.cat (K.M. Neyman), matolin@mbox.troja.mff.cuni.cz (V. Matolin).

http://dx.doi.org/10.1016/j.apcatb.2016.02.036
0926-3373/

A broad spectrum of physical vapour deposition (PVD) and surface coating techniques has been employed in the fabrication of various types of thin films (TF), but not yet in heterogeneous catalysis. This is because, until recently, the available PVD technologies were generally considered to be incompatible with the preparation of sufficiently large surface areas as required to achieve the desired catalytic activity. Recently we have developed a PVD (magnetron sputtering) process suitable for the preparation of high-surface-area nanoporous catalyst films. This method opens new ways to fast and cheap synthesis of large variety of catalytic nanomaterials. One key advantage of the TF technology is the wide range of achievable materials, which in many respects exceed those accessible by conventional preparation (wet techniques). A myriad of material combinations at many different compositions are accessible, e.g. in the form of composites, alloys, solid solutions, or mixed oxides. The variation of deposition parameters (such as substrate temperature, deposition rate and angle, type of reactive atmosphere, plasma treatment, simultaneous or sequential deposition, laser excitation, non-equilibrium growth, etc.) allows the cheap and environmentally friendly preparation of an exceptionally broad range of structures and materials, whose catalytic potential remains largely unexplored.

Materials based on Pt supported on cerium dioxide (ceria, CeO_2) have received a great deal of attention partly because of their widespread use in automobile catalytic converters, where pollutants from fuel combustion are transformed by means of the three-way catalysis [2,3]. In addition, catalysts consisting of finely dispersed Pt on a mixture of ceria and titania have shown remarkable activity for the water-gas-shift reaction, a key step for upgrading H_2 fuel [4]. For the PEMFC anode, we have recently designed a very metal-efficient Pt-CeO_2 material that meets the requirement of featuring atomically dispersed metal species that are sintering resistive [5–9]. Such material is based on nanoporous CeO_2 thin films prepared by simultaneous magnetron sputtering of Pt and CeO_2 [5,10–12]. This technique allows preparing oxide layers continuously doped with Pt atoms during growth. Spectroscopic characterization revealed that, in the systems thus prepared, Pt is mostly present either as cationic Pt^{2+} (on/near the surface) or as Pt^{4+} species (deeper inside ceria nanostructures) [5,7]. This finding strongly indicates that the atomically dispersed Pt cations on nanostructured ceria are involved in the FC anode catalysis rather than metallic particles which were believed to be essential for its activity. Combining Density Functional Theory (DFT) studies with Ultra-High Vacuum (UHV) surface science experiments we determined that such cationic Pt species consist of a structural element with unique properties: a surface Pt^{2+} cation that resides in a square-planar $[O^{2-}]_4$ coordination site located at {1 0 0} nanofacets of CeO_2 [9]. In addition, DFT calculations revealed that this structural unit is stable enough to withstand aggregation into metallic Pt nanoparticles (NPs). The unprecedentedly low Pt loading on the cheap cerium oxide support required for achieving significant catalytic activity makes this material of eminent economical interest. Furthermore, the activity of this novel and complex nanostructured catalyst cannot be rationalized using the models of platinum-catalysed hydrogen chemistry generally accepted up to date.

The most common problems for all types of FCs are the optimal design, stability, and durability of porous electrodes as well as investigation of the reaction mechanism and kinetics at each electrode/electrolyte interface. Therefore, the understanding of all these processes requires combination of theory with non-destructive experimental methods.

In this paper we show that the performance of the Pt-CeO_2 PEMFC anode can be substantially enhanced by using a new and commercially available carbon support consisting of highly dispersed carbon particles, the so-called nano-gas diffusion layer (nGDL) instead of previously used carbon nanotubes (CNTs) coated GDL [8]. In addition to the durability and higher performance reached by using nGDL, the fabrication of such PEMFC anode is simpler relative to the CNT based one. Furthermore, we show how the Pt loading of sputtered nanostructured Pt-CeO_2 coating affects the anode performance and that it is possible to find an ideal value of Pt loading that maximizes Pt efficiency. By means of X-ray Photoelectron Spectroscopy (XPS) and calculations based on DFT, we analyse the chemical state of the Pt content of the catalyst upon interaction with hydrogen, showing that Pt^{4+} cations are not stable and consequently not involved in the anode process. In turn, the more stable Pt^{2+} cations resist reduction to metallic Pt upon hydrogenation and are responsible for the catalyst activity.

2. Methods

2.1. Experimental details

2.1.1. Sample preparation

The magnetron sputtering was used to produce Pt-CeO_2 thin films. The catalyst layers were prepared by means of two magnetrons working simultaneously. Radio frequency (13.56 MHz) sputtering of ceria was performed by using a 2 inch diameter CeO_2 target installed on a TORUS 2" UHV magnetron (Kurt J. Lesker) with applied power of 50 W at distance of 90 mm from substrates. Pt was added by using the second DC homemade magnetron at the distance of 200 mm from substrates and tilted by 45° relative to the CeO_2 target, the power applied to the Pt target was 10 W. The sputtering was carried out in Ar atmosphere with total pressure of 4×10^{-1} Pa. The sputtering chamber was always evacuated up to 5×10^{-4} Pa before starting the deposition. The described sputtering conditions gave a growth rate of the Pt-doped cerium oxide films of 1 nm/min. We prepared and investigated three anode catalysts based on cerium oxide with different Pt contents of 0.6, 2 and 4 μg Pt/cm^2 of membrane electrode assembly (MEA) and the reference pure Pt film of 2 μg Pt/cm^2. All the samples were supported by the nGDL (SGL TECHNOLOGIES GmbH, Sigratec GDL 25 BC). The thickness of sputtered Pt-doped cerium oxide films was 30 nm. It was determined by Atomic Force Microscopy (AFM) as a thickness of the reference non-porous film deposited on the silicon substrate simultaneously. The Pt loading was calculated from the Pt-CeO_2 film thickness and Pt/Ce concentration ratio determined by means of quantitative XPS using the Pt 4*f* and Ce 3*d* spectra. This value was in a good agreement with Pt concentration obtained from known amounts of deposited Pt and ceria using calibrated deposition rates.

2.1.2. XPS

XPS measurements were carried out in an UHV experimental chamber operating at base pressures $<10^{-10}$ mbar and equipped with a SPECS Phoibos MDC 9 electron energy analyser and a dual Mg/Al X-ray source. However, for XPS measurements only Al K$\alpha_{1,2}$ anode was chosen (1486.6 eV, total energy resolution $\Delta E = 1$ eV) because the lower photon energy of the Mg K$\alpha_{1,2}$ X-ray source (1253.6 eV) would lead to higher and more inclined non-linear Ce 3*d* spectrum background and consequently to lower peak fitting precision.

2.1.3. FC performance tests

The FC tests were performed by using a device with pneumatically compressed graphite cell (Greenlight TP-5 Research Cell). We used MEA with an active area of 4.6 cm^2 formed from the 0.05 mm thick Nafion membranes (DuPont Inc., Nafion NR 212, perfluorosulfonic acid-PTFE copolymer), which was sandwiched by the catalyzed anode and cathode by pressing at 800 kPa. The nGDL support coated by 30 nm thick Pt-CeO_2 layer with different Pt loading between 0 and 4 μg of Pt/cm^2 has been used as a FC anode. The

cathode electrode was made by commercially available GDL supported Pt catalyst (Alfa Aesar, No. 45368, loading of Pt is 2 mg/cm^2). The cell was operated with pure humidified hydrogen as fuel and oxygen as oxidant under atmospheric pressure. The flow rates of H_2 and O_2 were controlled at 40 ml/min and 30 ml/min, respectively. The temperature of the cell was kept to be at 65 °C, the same as the temperature of both bubblers. The performance of the Pt doped cerium oxide as FC anode catalyst was evaluated by comparing it with a reference anode in a FC using MEA at the same working conditions. The used reference was a commercially available Pt/GDL anode (Alfa Aesar, No. 45367) with Pt loading of 2 mg Pt/cm^2.

2.1.4. Endurance tests

Durability of prepared catalyst films was tested by performing accelerated load cycling endurance test. During the test, a load giving 1 A/cm^2 was applied during 30 s and followed by 30 s of open circuit state generating open circuit voltage (OCV). Hydrogen treatment of the anode catalyst partially simulating the FC working condition was performed using a temperature and digital flow meter controlled flow reactor.

2.1.5. SEM and HRTEM

Morphology and structure of Pt-CeO_2/nGDL were explored by means of Scanning Electron Microscopy (SEM) using a Tescan MIRA 3 microscope operating at 30 keV electron beam energy and by Transmission Electron Microscopy (TEM) using the 200 kV JEOL 2100F microscope with a Scherzer resolution of 0.19 nm. The High Resolution TEM (HRTEM) images were recorded with an on-line charged coupled device camera, and the results were analysed using the Digital Micrograph software. The samples for TEM observation have been prepared by using Focus Ion Beam (FIB) (Tescan LYRA FIB-SEM) technique of thin lamellas cut from the catalyst films.

2.2. Computational details

The systems formed by atomically disperse cationic Pt and ceria nanocrystallites have been also investigated by means of spin-polarized density functional calculations. The same cuboctahedral $Ce_{40}O_{80}$ nanoparticle (NP) as in previous studies [13–16] has been used to model nanostructured ceria. This NP resulted from an exhaustive global optimization [14,15]. TEM measurements reveal the presence of ceria NPs ~5 nm large, while the NP model used in this work is 1.5 nm large. Despite the size difference, this $Ce_{40}O_{80}$ model is representative also of larger truncated cuboctaherdral NPs with different co-existing structural features. Namely, it retains the characteristic cubic fluorite type crystal structure (*Fm3m*) of CeO_2 bulk, and exposes O-terminated {1 1 1} and {1 0 0} facets and undercoordinated Ce and O atoms with larger structural flexibility. Furthermore, the O_4 square-planar sites of the (1 0 0) facets of ceria NPs, which are not present in extended surface models, are able to strongly anchor Pt^{2+} cations independently of the particle size [9].

In order to investigate cationic Pt on nanostructured ceria, we have substituted a single Pt atom for a Ce atom in different positions of the $Ce_{40}O_{80}$ NP (resulting in $PtCe_{39}O_{80}$) and examined the interplay between Pt^{4+}, Pt^{2+}, and metallic Pt^0 upon reduction processes. In particular, we have considered reduction of the model $PtCe_{39}O_{80}$ caused by both oxygen vacancy formation and dissociative H_2 adsorption. The adsorption energy of hydrogen $E_{ad}(H_2)$ is calculated per H_2 molecule as:

$$E_{ad}(H_2) = E(2H\text{-}PtCe_{39}O_{80}) - E(H_2) - E(PtCe_{39}O_{80}),$$

where $E(2H\text{-}PtCe_{39}O_{80})$, $E(H_2)$, and $E(PtCe_{39}O_{80})$ are the total calculated energies of the NP substrate hydrogenated by one dissociatively adsorbed H_2 molecule, the isolated H_2 molecule, and the non-hydrogenated substrate, respectively. The oxygen vacancy formation energy $E_f(O_{vac})$ is calculated as:

$$E_f(O_{vac}) = E(PtCe_{39}O_{79}) + \tfrac{1}{2}E(O_2) - E(PtCe_{39}O_{80}),$$

where $E(PtCe_{39}O_{79})$ and $E(O_2)$ correspond to the total calculated energies of the NP substrate with a single oxygen vacancy and of the isolated O_2 molecule (in the triplet state), respectively. Unfortunately, it is currently too computationally demanding to explicitly simulate the electrochemical conditions of the working fuel cell using DFT calculations. However, these two quantities ($E_f(O_{vac})$ and $E_{ad}(H_2)$) provide a first-principles rationale of the high stability of Pt^{2+} species on realistic models of nanostructured ceria upon different reductive processes.

We have used the PW91 exchange-correlation functional [17] corrected with an on-site Coulomb interaction term in the form of the Hubbard U (U = 4 eV) [18–20]. This approach is generally referred to as GGA + U or, more appropriately, PW91 + 4 for the particular combination of the functional and U parameter used in this work. The U correction offers a computationally feasible improvement to the incomplete cancellation of the self-interaction error affecting exchange-correlation functionals of the GGA family, which poorly describe strongly correlated systems. The approach used in the present work enables an appropriate treatment of systems featuring localized electrons in *d* or *f* orbitals and has been widely used to describe ceria-based systems [21,22] and ceria NPs in particular [13–16].

The GGA + U calculations have been carried out with the VASP code [23–25], using plane-wave basis sets with a kinetic energy cutoff of 415 eV to describe the valence states. The interaction between the core and valence states has been considered via the projector augmented wave method of Blöchl [26]. Since VASP is a periodic code, carrying out these GGA + U calculations requires placing the individual NPs in large enough unit cell, avoiding the interaction between the periodically repeated NPs. Accordingly, only the Γ-point has been used to sample the reciprocal space. A 10^{-4} eV total energy threshold defining self-consistent convergence was imposed and all studied geometric structures were optimized until forces acting on all atoms were smaller than 0.02 eV/Å.

The oxidation states of the Pt and Ce atoms resulting from the interaction of Pt with the ceria NP and from two different reductive processes (oxygen vacancy formation and dissociative H_2 adsorption) have been determined by the analysis of the localized magnetic moments on Ce cations: zero – for Ce^{4+} ($4f^0$) cations and close to unity – for Ce^{3+} ($4f^1$) cations.

3. Results

3.1. SEM and HRTEM

In this work we have investigated three ceria based anode catalysts prepared with different Pt contents of 0.6, 2 and 4 μg Pt/cm^2 of MEA, denoted as 0.6-Pt/Ce, 2-Pt/Ce and 4-Pt/Ce, respectively, and the sputtered reference pure Pt film of 2 μg Pt/cm^2 (labelled as 2-Pt). Pt loading per 1 cm^2 of the anode was calculated from determined platinum concentrations, see Experimental details. The Pt-CeO_2 30 nm thick thin film catalysts as well as the reference Pt film were deposited on the nGDL support with carbon nanoparticles of 50–80 nm in size on the surface as can be seen from the SEM image in Fig. 1(a). These carbon particles form conglomerates ensuring large specific surface of the nGDL substrate and a good diffusion of the gas feed to the catalyst film. Fig. 1(b) shows details of the surface of the nGDL covered by the catalyst layer. The catalyst film reveals enhanced porosity relative to the bare nGDL substrate which is in agreement with results of cerium oxide sputtering on different carbon substrates [5,8,10–12,27]. Recently we

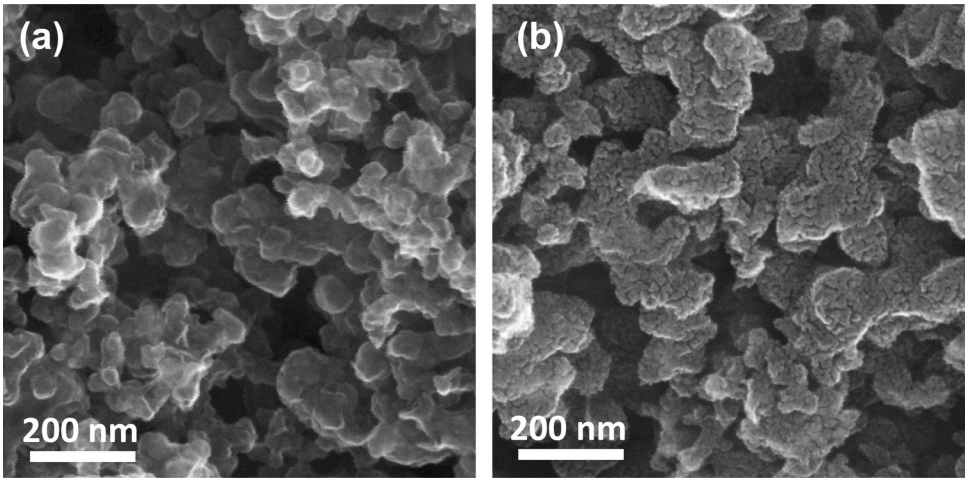

Fig. 1. SEM images of the nGDL without (a) and with Pt-CeO_2 coating (b).

rationalized the mechanism of the porous structure growth by carbon substrate etching by oxygen plasma [10,11] produced by RF ionization of oxygen released from the sputtering target and/or of oxygen added to the working gas. This behaviour makes the deposited thin film suitable for catalytic applications.

TEM observation confirmed nanostructural character of magnetron sputtered films containing ceria crystallites of 2–5 nm in size. Fig. 2 provides an example of HRTEM images of the Pt doped cerium oxide catalysts 2-Pt/Ce and 4-Pt/Ce, respectively. It shows atomic resolution pictures of the cerium oxide nanoparticle lattice in {1 1 0} plane. It can be seen that the surface of NPs exhibits {1 1 1} × {1 0 0} facets which have been shown to expose specific sites anchoring atomically dispersed ionic Pt^{2+} [9]. Notably, HRTEM images did not show any traces of Pt or Pt oxide particles in thin films of ceria with low Pt loadings.

3.2. Performance tests

The polarization *I–V* curves measured on all prepared anode catalysts are shown in Fig. 3 together with the corresponding power density (PD). PD was determined relative to unit of geometrical surface of MEA. We also performed in-situ electrochemical surface analysis (ECSA) by determining charge from the hydrogen adsorption on anode, 1.9 mC/cm^2 in case of the 2 μg Pt in CeO_2/cm^2 catalyst. However, we could not determine active Pt surface because the catalyst did not have character of metallic Pt. Moreover, we still do not know if Pt is the only active component of the catalyst, see Discussion part below.

Comparing PD values in Fig. 3 one can see that maximum PD for ceria based catalysts was obtained for the 2-Pt/Ce (2 μg Pt in CeO_2/cm^2) catalyst, whilst higher and lower Pt loadings gave rise to lower efficiency. We note that we also tested pure cerium oxide film which gave negligible FC current. By knowing PD and Pt loading per 1 cm^2 of MEA we can calculate specific power (SP) representing power delivered per 1 g of Pt, i.e. activity per unit of mass. This quantity expresses the Pt efficiency of the catalyst and is therefore related to its cost.

Maximum power density PD as well as calculated values of specific power for all the measured catalysts are presented in Fig. 4. Thus, the maximum power density PD = 0.41 W/cm^2 among the different Pt/ceria catalysts was obtained for the 2-Pt/Ce catalyst, which corresponds to very high specific power $SP_{(2\text{-Pt/Ce})}$ = 205 kW/g(Pt) at small Pt loading of 2 μg/cm^2.

In Fig. 3 we also show the results of two reference PEMFC experiments performed at the same FC conditions using the same cathode catalyst, but replacing the Pt-CeO_2/nGDL by the sputtered pure platinum 2-Pt catalyst and the standard commercial Pt catalyst (2 mg Pt ref). By considering the given loading of Pt in the commercial reference, we obtain the corresponding maximum $SP_{(2\text{ mg Pt ref})}$ = 0.22 kW/g(Pt). Thus, we can see that in spite of only 1.1 times higher maximum $PD_{(2\text{ mg Pt ref})}$ in case of the reference MEA relative to the $PD_{(2\text{-Pt/Ce})}$ value, the specific power obtained for the 2-Pt/Ce anode was three orders of magnitude higher due

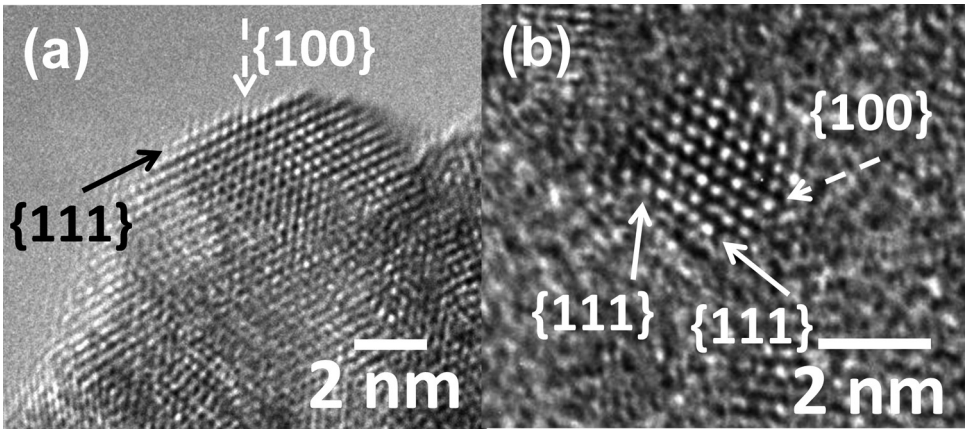

Fig. 2. HRTEM images of the Pt doped cerium oxide catalysts: 2-Pt/Ce (a) and 4-Pt/Ce (b). The CeO_2 {111} and {1 0 0} facets are marked by arrows.

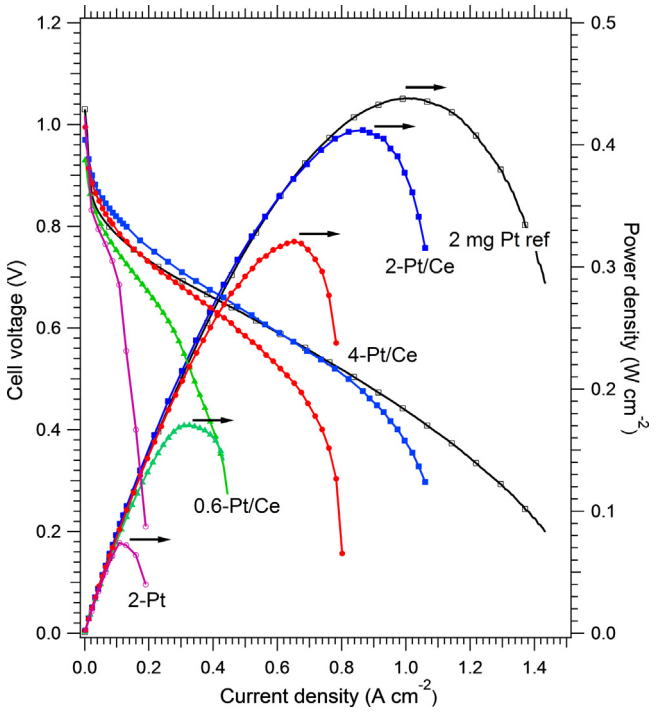

Fig. 3. The polarization *I–V* curves (left Y-axis) and the corresponding power density (right Y-axis) measured for the three ceria based anode catalysts prepared with different Pt contents of 0.6, 2 and 4 μg Pt/cm^2 of MEA (the samples denoted 0.6-Pt/Ce, 2-Pt/Ce and 4-Pt/Ce), and the sputtered reference pure Pt film of 2 μg Pt/cm^2 (2-Pt), all deposited on the nGDL. For comparison the data obtained on the commercial Pt/GDL catalyst (2 mg Pt ref) are added.

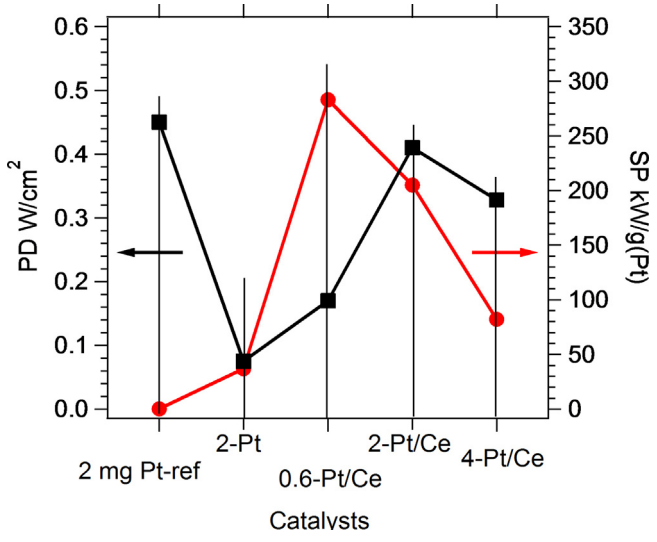

Fig. 4. Maximum power density PD (left Y-axis) and specific power SP (right Y-axis) for all the catalysts data presented in Fig. 3.

to high activity and very low Pt loading. We note that, for the PEMFC Pt anode catalysts, Pt loading can be significantly decreased [28] relative to the reference electrode we used. Presently used state-of the art anodes contain around 0.3 mg of Pt/cm^2. Nevertheless, the nGDL supported Pt-CeO_2 thin film catalysts reported here still exhibit unprecedentedly high mass activity which outperforms even such state-of-the-art catalysts. Comparing with our previous results obtained for similar Pt-ceria films deposited on CNTs [7] (PD_{max} = 74 mW/cm^2 at 75 °C), we can see that by using the nGDL support we further increased the anode power density, which became well comparable with that of the commercial catalysts.

Table 1
Maximum specific power SP, power density PD and PD × SP product.

Anode catalyst	SP (kW/g Pt)	PD (W/cm^2)	PD × SP(arb. u.)
0.6-Pt/Ce	283	0.17	57.3
2-Pt/Ce	205	0.41	100
4-Pt/Ce	82	0.33	32.3
2-Pt	37	0.075	3.3
2 mg Pt-ref	0.22	0.44	0.1

In Fig. 4 we compared the activity of anodes loaded with the three different Pt contents in cerium oxide and pure Pt reference anode prepared by sputtered deposition containing 2 μg Pt/cm^2 (2-Pt). If we consider PD × SP product as a parameter reflecting economical suitability of the catalyst for practical use, i.e. activity per cost (SP is inversely proportional to the cost), we find that platinum doped cerium oxide is superior to pure Pt. The PD, SP and relative values of PD × SP are compared in Table 1.

3.3. Durability test

The 2-Pt/Ce MEA durability test was performed by using load cycling of 6000 cycles of 30 s of high current density (1 A/cm^2) followed by 30 s of open circuit state. During the test I–V FC characteristics were measured after each 300 cycles. Obtained maximum PD are plotted in Fig. 5 showing excellent stability of the ionic Pt doped cerium oxide catalyst during the whole test. It can be considered as an indirect proof of both good structural and chemical stability of the catalyst during the test.

3.4. XPS

Now we focus on the chemical state of Pt in the Pt/CeO_2 catalysts. We used XPS of Pt 4*f* states to compare four catalysts: 0.6-Pt/Ce, 2-Pt/Ce, 4-Pt/Ce and 2-Pt. The XPS Pt 4*f* spectra of the as-deposited catalyst films are plotted in Fig. 6(a). All spectra of ceria-based catalysts exhibit two $4f_{7/2}$–$4f_{5/2}$ doublets at binding energies (BEs)\ of 72.5–75.8 eV and 74.2–77.5 eV corresponding to Pt^{2+} and Pt^{4+} species, respectively [5]. The relative intensities of the Pt^{2+} and Pt^{4+} peaks in Pt 4*f* spectra can be used to calculate the Pt^{2+}/Pt^{4+} ratios, giving 0.70, 1.21 and 2.15 for the 4-Pt/C, 2-Pt/C and 0.6-Pt/Ce catalysts, respectively. These results show that lower Pt loadings lead to higher relative abundance of Pt^{2+} species in the sputtered Pt-CeO_2 films. In contrast and as expected, the pure Pt film (2-Pt) contains only metallic platinum, which is identified by its characteristic doublet at BEs 71.2–74.5 eV and an asymmetric shape of the Pt 4*f* peaks.

Cerium dioxide and platinum oxide are a reducible oxides, and one can expect that the Pt-Ce-O mixed oxide would then be susceptible to reduction by hydrogen. In addition, in the PEMFC anode, water vapour is mixed with the hydrogen feed due to the necessity of keeping the proton-exchange membrane wet. In order to assess the effect of such conditions on the anode catalyst, we tested the nGDL-supported Pt-CeO_2 catalyst films (identical to those used for the FC test in Fig. 3) in the flow reactor by simulating anode conditions of the PEMFC operation. The cerium oxide catalysts were thus heated in the humidified hydrogen flow of 30 ml/min at 65 °C for 24 h (hydrogen was humidified by bubbling through water). Fig. 6(b) shows the Pt 4*f* spectra of the catalyst films recorded after such annealing process. The differences between the Pt 4*f* spectra for the catalyst films as-prepared and after simulation of the anode conditions shown in Fig. 6(a) and (b) indicate that after wet hydrogen annealing the Pt^{4+} species disappear. In case of low Pt loading (0.6 and 2 μg Pt/cm^2 of MEA), the annealing results in Pt^{2+} as the only Pt state present, whilst for the 4-Pt/Ce sample the disappearance of Pt^{4+} is concomitant with the formation of more Pt^{2+} and Pt^0,

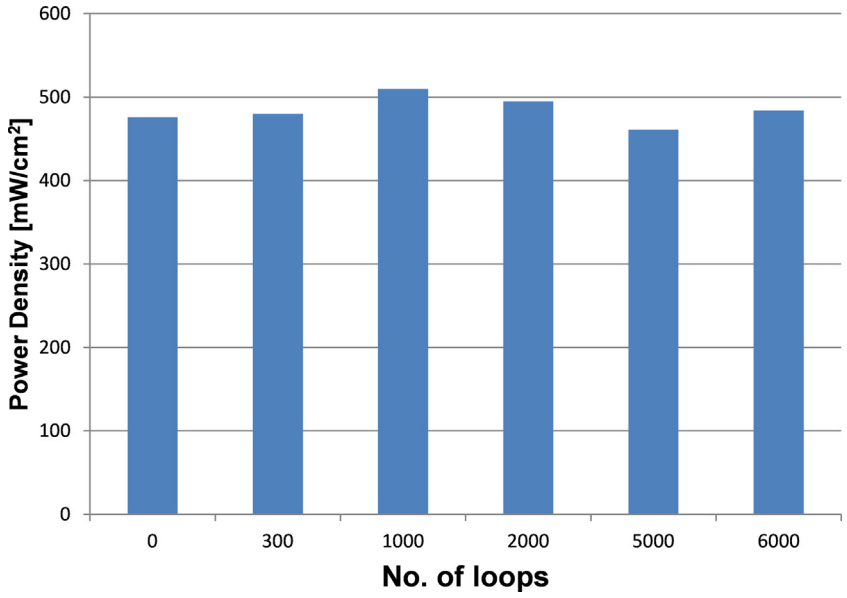

Fig. 5. Durability test of the 2-Pt/Ce catalyst. Maximum power density is plotted versus number of cycles.

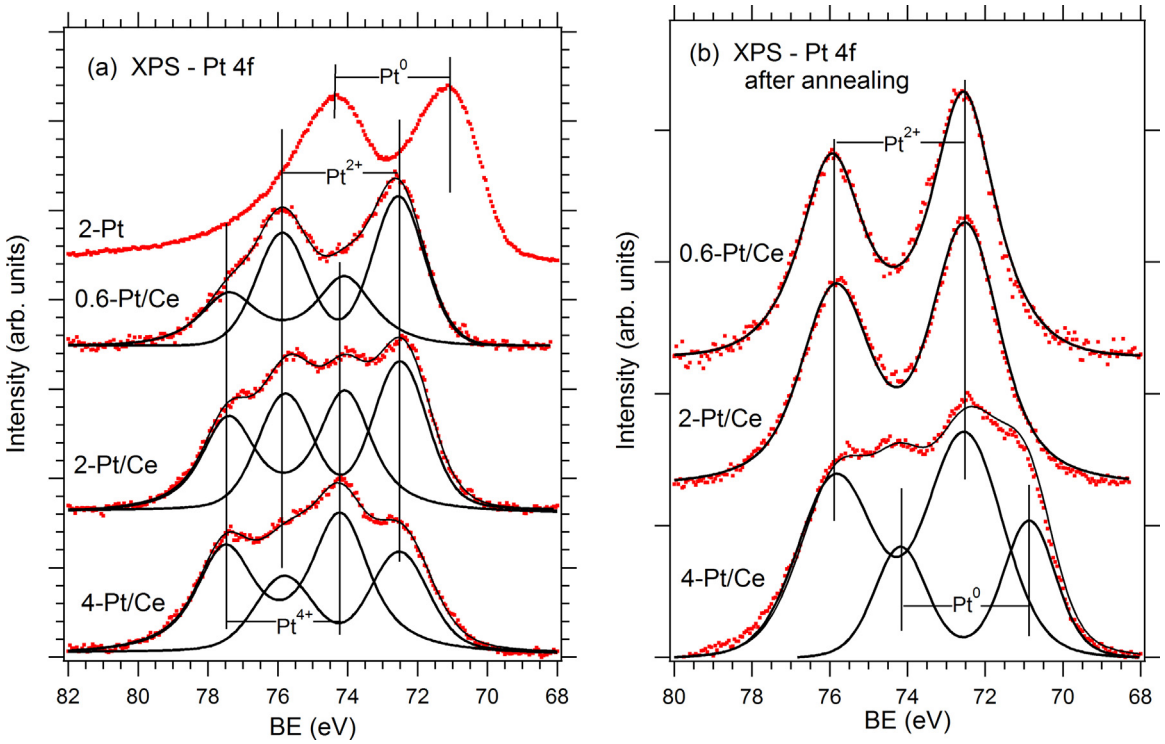

Fig. 6. XPS Pt 4*f* spectra of the sputtered reference pure Pt film of 2 μg Pt/cm^2 (the sample 2-Pt) and the three ceria based anode catalysts with different Pt contents of 0.6, 2 and 4 μg Pt/cm^2 of MEA (the samples denoted 0.6-Pt/Ce, 2-Pt/Ce and 4-Pt/Ce) as-prepared (a) and after wet hydrogen annealing simulating anode conditions of the PEMFC operation (b). All the catalysts films were sputter deposited on the nGDL.

resulting in a Pt^{2+}/Pt^0 ratio of 1.65. This clearly shows that Pt^{4+} is not a stable component under the FC operating conditions, while Pt^{2+} and Pt^0 are stable even after the sample transfer in air. Although the exposure to H_2 cannot fully simulate the operation conditions of the catalyst in the PEMFC, this test suggests that sputtered Pt-ceria catalysts with higher Pt loading (above 2 μg Pt/cm^2 in this case) are composed of ionic and metallic Pt.

3.5. DFT modelling

In order to further characterize the relative stability and interplay between the Pt^{4+} and Pt^{2+} species upon different reduction processes, we have performed DFT calculations modelling the Pt-doping of a ceria NP (Fig. 7). By stoichiometry, the substitution of Pt for Ce results in formally Pt^{4+} cations, which are energetically stabilized by the subsequent diffusion from the inner (bulk) posi-

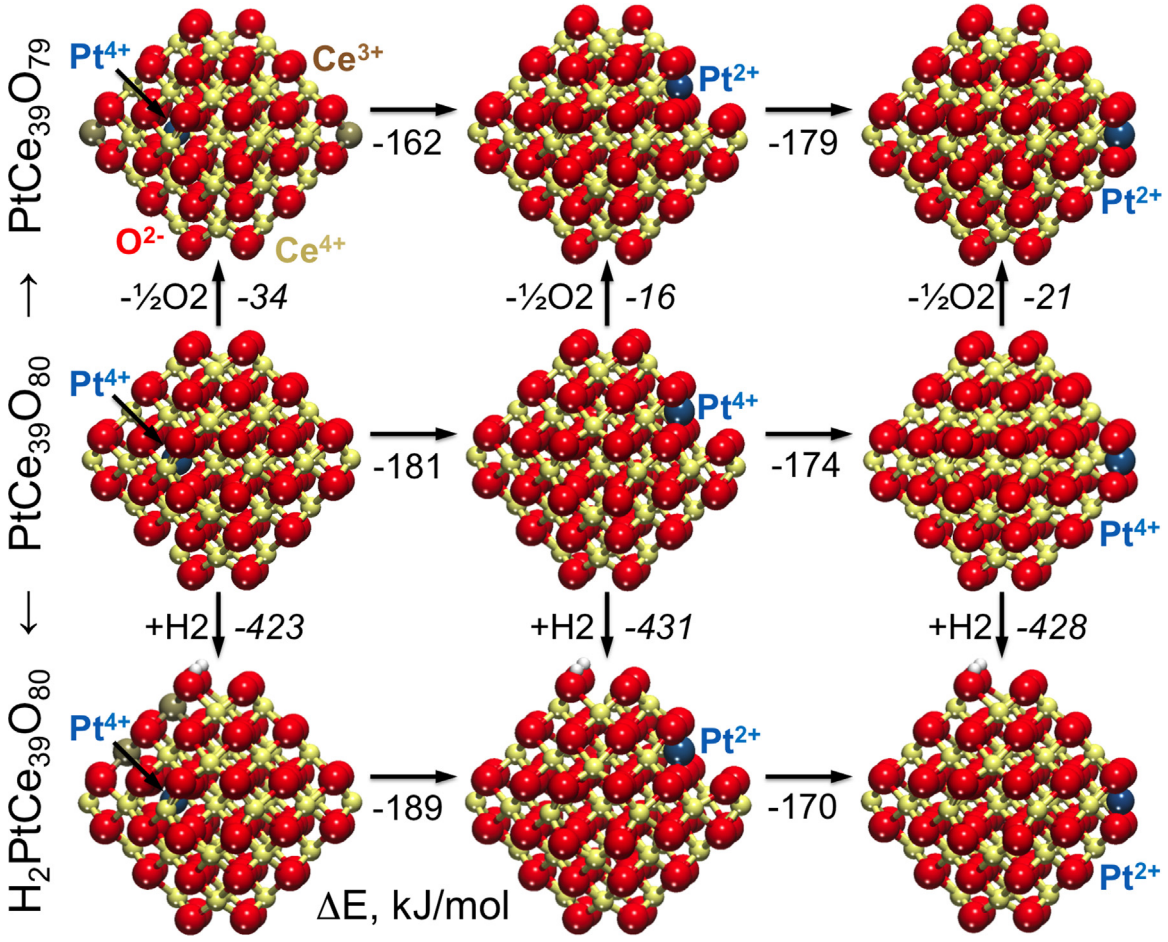

Fig. 7. Structures and stability of ceria NPs doped with a Pt atom in selected inner and surface cationic positions. Middle row – substitution of Ce by Pt in a pristine NP $Ce_{40}O_{80}$, resulting in $PtCe_{39}O_{80}$; upper row – the corresponding systems $PtCe_{39}O_{79}$ with the oxygen vacancy in the position calculated to be energetically most favourable in the pristine NP (in the {1 0 0} facet); bottom row – the corresponding systems with dissociatively adsorbed H_2 molecule on the most favourable surface O sites, $H_2PtCe_{39}O_{80}$. White, blue, red, beige, and brown spheres depict H, Pt, O, Ce^{4+}, and Ce^{3+}, respectively. (For interpretation of the references to colour in this figure legend, the reader is referred to the web version of this article.)

tions of ceria NPs to the surface. This is clearly indicated by the relative energies of the Pt-doped systems with Pt either at inner or surface positions of the ceria NP (Fig. 7–middle row). In addition, all these doped systems appear to be slightly energetically unstable with respect to their reduced forms with the spontaneous release of one O atom from the {1 0 0} facets (and possibly from other positions as well). Removing a single O atom from such site, which is the most stable position for the formation of an oxygen vacancy, O_{vac}, in the pristine NPs such as $Ce_{40}O_{80}$ results in negative vacancy formation energies for each Pt-doped case considered (Fig. 7–upper row). This contrasts with the 79 kJ/mol necessary to remove the same O atom in absence of a doping Pt atom [14]. The differences in $E_f(O_{vac})$ between undoped and Pt-doped systems can be traced back to the origin of species which are reduced upon formation of the oxygen vacancy. Thus, in the presence of surface Pt^{4+} species, the two electrons left behind by the formation of the oxygen vacancy induce a Pt reduction from 4+ to the 2+ state, whereas for the bare ceria NP, two Ce^{4+} cations are reduced to Ce^{3+} instead.

The dissociative adsorption of H_2 molecules is a reduction process taking place under the working conditions of anode FC catalysts. This process gives rise to the formation of OH groups and to the donation of 2 electrons per H_2 molecule to the NP, which can also cause the reduction of either surface Pt^{4+} or Ce^{4+} cations. Analogously to the reduction by formation of oxygen vacancies, the two electrons from the dissociative adsorption of H_2 reduce surface Pt^{4+} to Pt^{2+} (Fig. 7–bottom row). The resulting adsorption energies are also larger (in magnitude) than for the undoped NP, which is again due to the more facile reducibility of Pt^{4+} species with respect to Ce^{4+}.

Interestingly, neither the oxygen vacancy formation nor the dissociative adsorption of H_2 reduces the Pt^{4+} cations when these occupy inner (bulk) positions of the NPs. In these cases, the two electrons reduce two Ce^{4+} cations to Ce^{3+} instead. Bulk-like Pt^{2+} species are formed when generating an oxygen vacancy in a neighbouring position to a bulk-like Pt^{4+} cation, following the mechanism described by Scanlon et al. [29]. Nevertheless, the removal of an O atom from the {1 0 0} nanofacet, which reduces Ce^{4+} cations and does not distort the coordination environment of Pt^{4+}, is preferred by 11 kJ/mol. Furthermore, the partially reduced systems with Pt^{4+} species in bulk positions are significantly less stable than the corresponding systems with Pt^{2+} species at the surface (Fig. 7–upper and bottom rows). Thus, upon reduction, one would expect Pt^{2+} species to be formed from Pt^{4+} ones and exposed mainly on the surface of ceria NPs. This explains the disappearance of Pt^{4+} species detected by XPS upon annealing the Pt-doped ceria catalysts under H_2 flow. Note that the most stable location of Pt^{2+} species is at the NP corner, where in the undoped system Ce^{4+} cation interacted with four O anions of the so-called $\{O_4\}$ pocket. The local, very slightly distorted square-planar O structure around these Pt^{2+} species ($r(Pt\text{-}O) = 204 \div 205$ pm, $\angle O\text{-}Pt\text{-}O = 89 \div 91^\circ$) is basically identical to that formed by adsorbed Pt atoms in the $\{O_4\}$ pockets on stoichiometric ceria

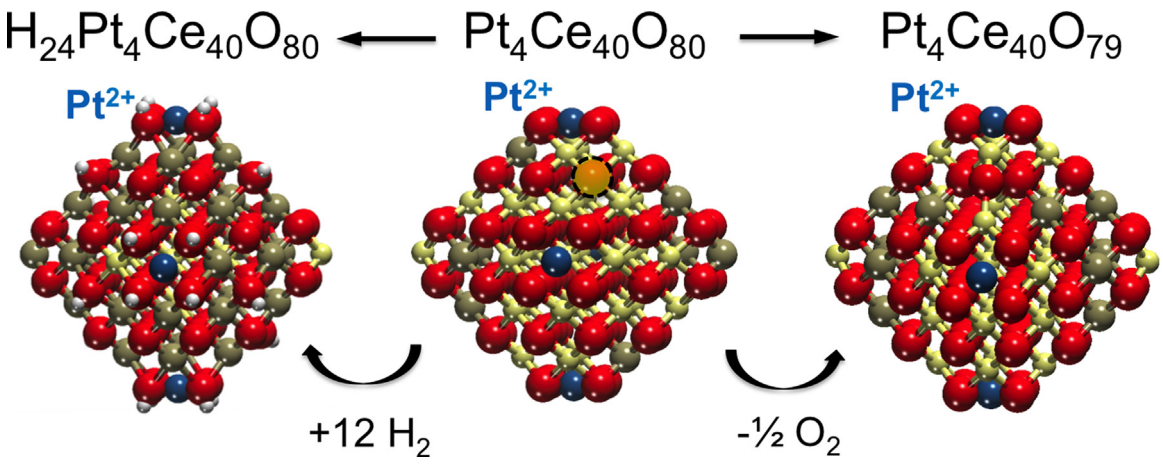

Fig. 8. Structure of the $Pt_4Ce_{40}O_{80}$ model with 4 Pt atoms in the 2+ state (center). 24 Ce^{4+} cations are reduced to the Ce^{3+} state upon dissociative adsorption of 12 H_2 molecules (left) resulting in $E_{ad}(H_2)$ = 156 kJ/mol per H_2 molecule. Nevertheless, the four atomic Pt^{2+} species retain their oxidation state and very strong bonding to the ceria substrate. Note that the adsorption of 24 H and 4 Pt leads to the reduction of 32 Ce^{4+} to Ce^{3+} state. The removal of an oxygen atom to form $Pt_4Ce_{40}O_{79}$ (right) results in a dramatic increase of the vacancy formation energy ($E_f(O_{vac})$ = 210 kJ/mol) with respect to the bare $Ce_{40}O_{80}$ NP ($E_f(O_{vac})$ = 79 kJ/mol). Color-coding is the same as in Fig. 7 and position of the O atoms removed is indicated by a circle.

NPs (r(Pt-O) = 205 pm, ∠O-Pt-O = 90°). Interestingly, in the other positions of Pt^{2+} species displayed in Fig. 8 the local structure clearly tends to be square-planar (r(Pt-O) = 202 ÷ 204 pm, ∠O-Pt-O = 86 ÷ 93°) and its formation causes visible deformations of the NP. This illustrates how the presence of Pt atoms in strong contact with ceria NPs can lead to larger abundance of {1 0 0} nanofacets exposing the PtO_4 surface complexes.

The remarkable resistance of the Pt^{2+} species in our Pt^{2+}/ceria nanomaterials to the reduction by hydrogen (i.e. under typical FC working conditions) has already been addressed by means of DFT modelling in previous work [9]. Here, we extend the study to larger coverage of adsorbed Pt with all four $\{O_4\}$ coordination positions of the model ceria NP occupied by Pt^{2+} species and the surface densely covered by adsorbed hydrogen atoms (Fig. 8). Even for 24 H atoms accommodated on O atoms of the $Pt_4Ce_{40}O_{80}$ system, the adsorbed Pt species remain strongly bound in the 2+ state, while 24 Ce^{4+} cations are reduced to the Ce^{3+} state. This is in excellent agreement with the present observations of exceptionally high stability of our Pt^{2+}/ceria FC catalysts under working conditions (vide supra). In addition, the presence of Pt^{2+} cations in the {1 0 0} facets of the ceria NP hinders the formation of oxygen vacancies. The under-coordinated O atoms of such facets in the case of the bare ceria NP are easily removable ($E_f(O_{vac})$ = 79 kJ/mol). Nevertheless, when these O atoms are coordinated to Pt^{2+} cations, their removal is dramatically hindered and generating an oxygen vacancy in a different position is preferred resulting in $E_f(O_{vac})$ = 210 kJ/mol. Thus, although doping nanostructured ceria with Pt initially leads to the formation of spontaneous charge compensating oxygen vacancies that reduce surface Pt^{4+} cations, the strength of the Pt^{2+}-O bonds prevents the formation of additional vacancies.

4. Discussion

The results of this work have shown that the preparation of thin film nanomaterials represents a new way for designing novel and cost-efficient active catalysts. In particular, we have prepared Pt-containing PEMFC anode catalysts exhibiting very high Pt-efficiency by coating a large surface area substrate composed of a conglomerate of carbon nanoparticles with Pt-doped cerium oxide thin films (30 nm in this case). The XPS spectra of such thin film nanomaterials reveal that the chemical state of Pt is intimately related to the amount of Pt present in the thin film. Low Pt loadings (corresponding to the 0.6-Pt/Ce and 2-Pt/Ce samples) give nanocomposites with Pt species in the 2+ state only. Nevertheless, further increase of the Pt content (4-Pt/Ce sample) leads to the presence of metallic Pt species reflecting the limited concentration of sites that can accommodate Pt^{2+} in a square-planar coordination of O atoms. These structural units have been fully characterized by DFT modelling and are exposed at {1 0 0} facets of ceria, which are also detected on the nanostructured thin film catalysts presented in this work by HRTEM imaging (Fig. 2). The ceria NP model used in this work exhibits 4 such anchoring sites (or 6 if we also consider the substitutions of corner Ce atoms by Pt atoms), and once these are occupied by Pt^{2+} species (as in the model presented in Fig. 8), additional Pt atoms would adsorb in metallic form.

The 0.6-Pt/Ce and 2-Pt/Ce catalysts present relatively high power density, which together with the small Pt loadings required for fabricating them, results in very high SP. In addition, the PD is larger for the 2-Pt/Ce catalyst than for the 0.6-Pt/Ce one, which indicates that larger concentration of Pt^{2+} species involves greater electrocatalytic activity. In turn, the presence of metallic Pt in the 4-Pt/Ce sample results in a ~25% drop in PD and to an even more significant drop in specific power of >50%. The reason of such decrease of PD with increasing Pt content remains unclear. It is possible that formation of Pt clusters leads to a decrease in both catalyst porosity and electrochemically active surface and/or to partial blocking of ceria sites accommodating ionic Pt. Investigation of these phenomena is subject of our further research. Nevertheless, in spite of lack of understanding, this work shows that ionic Pt^{2+} is a key species for the high activity of Pt-ceria thin film catalysts.

We have established that Pt^{2+} is necessary for achieving high electrocatalytic activity and specific power in the PEMFC. Nevertheless, the mechanisms by which the beneficial effects of Pt^{2+} operate remain not clear. Metal-free hydrogenation activity on ceria has been reported at higher pressures [30,31] which indicates that hydrogen dissociation can occur on ceria samples without Pt under the appropriate conditions. In addition, metallic Pt favours the degradation of nanostructured ceria through oxygen spill-over processes [16], whereas strongly bound Pt^{2+} species hinder the removal of O atoms from the Pt^{2+}-O_4 complex and are also very resistant to reduction by H_2. Thus, under the operation conditions of PEMFC catalysts, i.e. at high pressures and low temperatures, Pt^{2+} might not directly participate in H_2 dissociation, and its role could then be mainly limited to avoiding the degradation of nanostructured ceria. One can expect that without Pt^{2+} species the facile creation of abundant oxygen vacancies on ceria NPs would

cause significant structural degradation of the material. In addition, highly reduced ceria would have fewer available O atoms for the formation of surface hydroxyls and fewer Ce^{4+} centres that can be reduced to Ce^{3+}. Another possibility is that Pt^{2+} species lead to greater abundance of certain terminations of cerium oxide such as the {1 0 0}, whose larger surface energy than (1 1 1) or (1 1 0) terminations is greatly reduced by stabilization upon adsorption of Pt^{2+}. At last, we do not discard the possibility that the catalysts are somehow transformed under reaction conditions into a form that is particularly favourable for the electrocatalytic process [32].

5. Conclusions

In summary, we have designed a family of novel cost-efficient PEMFC anode catalysts by sputtering ceria thin films with low Pt loadings on a nanostructured carbon support. By combining XPS spectroscopy and catalytic performance analysis, we have determined that the presence of Pt^{2+} species is crucial for achievement of the electrocatalytic activity. DFT calculations suggest that the great stability of Pt^{2+} species on ceria makes these resistant to reduction by hydrogenation and that the formation of such stable surface complexes prevents degradation of the nanostructured composite. Remarkably, only small amounts of surface Pt^{2+} species are necessary for achieving power density values comparable to the reference commercial catalysts, which results in excellent specific activities of our samples. In spite of the typically lower Pt loading required for the hydrogen oxidation reaction, the decrease in Pt loading at the anode electrocatalyst represents significant savings for MEA production.

Acknowledgements

The authors acknowledge financial support by the European Commission (FP7-NMP.2012.1.1-1 project ChipCAT, Reference No. 310191), the Czech Science Foundation(grant 13-10396S) and the Czech Ministry of Education under the project LD13054. The theoretical part of the work has been supported by Spanish MINECO (grants CTQ2012-34969 and CTQ2015-64618-R) and the Generalitat de Catalunya (grants 2014SGR97 and XRQTC). The authors also thank the COST Action CM1104 for additional support. Computer resources and assistance were provided by the Red Española de Supercomputación and Agence Nationale de la Recherche within IMAGINOXE project (ANR-11-S10-001). J.L. thanks the support of Conseil Régional de Bourgogne (PARI ONOV 2012). AB acknowledges support from the European Research Council under the European Union's Seventh Framework Programme (FP/2007-2013)/Marie Curie Actions/Grant no. 626764 (NanoDeSign). RF acknowledges support from the Charles University grant No.942214.

References

[1] Q. Fu, H. Saltsburg, M. Flytzani-Stephanopoulos, Science 301 (2003) 935–938.
[2] H.S. Gandhi, G.W. Graham, R.W. McCabe, J. Catal. 216 (2003) 433–442.
[3] M. Hatanaka, N. Takahashi, T. Tanabe, Y. Nagai, A. Suda, H. Shinjoh, J. Catal. 266 (2009) 182–190.
[4] A. Bruix, J.A. Rodriguez, P.J. Ramírez, S.D. Senanayake, J. Evans, J.B. Park, D. Stacchiola, P. Liu, J. Hrbek, F. Illas, J. Am. Chem. Soc. 134 (2012) 8968–8974.
[5] V. Matolin, I. Matolinova, M. Vaclavu, I. Khalakhan, M. Vorokhta, R. Fiala, I. Pis, Z. Sofer, J. Poltierova-Vejpravova, T. Mori, V. Potin, H. Yoshikawa, S. Ueda, K. Kobayashi, Langmuir 26 (2010) 12824–12831.
[6] V. Matolin, US Patent 8435921, 2013.
[7] V. Matolin, M. Cabala, I. Matolinova, M. Skoda, M. Vaclavu, K.C. Prince, T. Skala, T. Mori, H. Yoshikawa, Y. Yamashita, S. Ueda, K. Kobayashi, Fuel Cells 10 (2010) 139–144.
[8] R. Fiala, I. Khalakhan, I. Matolinova, M. Vaclavu, M. Vorokhta, Z. Sofer, S. Huber, V. Potin, V. Matolin, J. Nanosci. Nanotechnol. 11 (2011) 5062–5067.
[9] A. Bruix, Y. Lykhach, I. Matolínová, A. Neitzel, T. Skála, N. Tsud, M. Vorokhta, V. Stetsovych, K. Ševčíková, J. Mysliveček, R. Fiala, M. Vaclavu, K.C. Prince, S. Bruyere, V. Potin, F. Illas, V. Matolin, J. Libuda, K.M. Neyman, Angew. Chem. Int. Ed. Engl. 53 (2014) 10525–10530.
[10] M. Dubau, J. Lavkova, I. Khalakhan, S. Haviar, V. Potin, V. Matolin, I. Matolinova, ACS Appl. Mater. Interfaces 6 (2014) 1213–1218.
[11] S. Haviar, M. Dubau, J. Lavkova, I. Khalakhan, V. Potin, V. Matolin, I. Matolinova, Sci. Adv. Mater. 6 (2014) 1278–1285.
[12] J. Lavkova, I. Khalakhan, M. Chundak, M. Vorokhta, V. Potin, V. Matolin, I. Matolinova, Nanoscale 7 (2015) 4033–4047.
[13] G.N. Vayssilov, A. Migani, K.M. Neyman, J. Phys. Chem. C 115 (2011) 16081–16086.
[14] A. Migani, G.N. Vayssilov, S.T. Bromley, F. Illas, K.M. Neyman, Chem. Commun. 46 (2010) 5936–5938.
[15] A. Migani, G.N. Vayssilov, S.T. Bromley, F. Illas, K.M. Neyman, J. Mater. Chem. 20 (2010) 10535–10546.
[16] G.N. Vayssilov, Y. Lykhach, A. Migani, T. Staudt, G.P. Petrova, N. Tsud, T. Skála, A. Bruix, F. Illas, K.C. Prince, V. Matolín, K.M. Neyman, J. Libuda, Nat. Mater. 10 (2011) 310–315.
[17] J.P. Perdew, Y. Wang, Phys. Rev. B: Condens. Matter 45 (1992) 13244–13249.
[18] V.I. Anisimov, F. Aryasetiawan, A.I. Lichtenstein, J. Phys.: Condens. Matter 9 (1997) 767.
[19] V.I. Anisimov, I.V. Solovyev, M.A. Korotin, M.T. Czyzyk, G.A. Sawatzky, Phys. Rev. B: Condens. Matter 48 (1993) 16929–16934.
[20] I.V. Solovyev, P.H. Dederichs, V.I. Anisimov, Phys. Rev. B: Condens. Matter 50 (1994) 16861–16871.
[21] C. Loschen, J. Carrasco, K. Neyman, F. Illas, Phys. Rev. B 75 (2007), 035115.
[22] J. Paier, C. Penschke, J. Sauer, Chem. Rev. 113 (2013) 3949–3985.
[23] G. Kresse, J. Hafner, Phys. Rev. B: Condens. Matter 47 (1993) 558–561.
[24] G. Kresse, J. Furthmüller, Phys. Rev. B: Condens. Matter 54 (1996) 1169–1186.
[25] G. Kresse, J. Furthmüller, Comput. Mater. Sci. 6 (1996) 15–50.
[26] P.E. Blöchl, Phys. Rev. B: Condens. Matter 50 (1994) 17953–17979.
[27] I. Khalakhan, M. Dubau, S. Haviar, J. Lavkova, I. Matolinova, V. Potin, M. Vorokhta, V. Matolin, Ceram. Int. 39 (2013) 3765–3769.
[28] H.A. Gasteiger, J.E. Panels, S.G. Yan, J. Power Sources 127 (2004) 162–171.
[29] D.O. Scanlon, B.J. Morgan, G.W. Watson, Phys. Chem. Chem. Phys. 13 (2011) 4279–4284.
[30] G. Vilé, B. Bridier, J. Wichert, J. Pérez-Ramírez, Angew. Chem. Int. Ed. Engl. 51 (2012) 8620–8623.
[31] G. Vilé, S. Colussi, F. Krumeich, A. Trovarelli, J. Pérez-Ramírez, Angew. Chem. Int. Ed. Engl. 53 (2014) 12069–12072..
[32] Y. Lykhach, A. Figueroba, M.F. Camellone, A. Neitzel, T. Skála, F.R. Negreiros, M. Vorokhta, N. Tsud, K.C. Prince, S. Fabris, K.M. Neyman, V. Matolín, J. Libuda, Phys. Chem. Chem. Phys. 18 (2016), http://dx.doi.org/10.1039/c6cp00627b.